Original Paper

Implications for a Geothermal Reservoir at Abgarm, Mahallat, Iran: Magnetic and Magnetotelluric Signatures

Seyed Hossein Hosseini,[1] Banafsheh Habibian Dehkordi,[1] Maysam Abedi,[2,3] and Behrooz Oskooi[1]

One of the well-known geothermal potential areas in Iran is the Abgarm in Mahallat region. Due to existence of several hot springs, the Abgarm area is of particular importance in geothermal studies. To investigate the geothermal mechanism at Abgarm, geophysical surveys of magnetometry and magnetotelluric (MT) were utilized near hot springs to image the geometry of all geological requisites for trapping a geothermal reservoir. The ground magnetic data were inverted in 3D to construct a magnetic susceptibility model, where a deep intrusive igneous rock (as a heat source) and a shallow magmatic lava were inferred from the physical model. Euler depth estimation also provided insight to a shallow granodiorite unit embedded in a thick sequence of sediments. Dimensionality and strike analysis of the MT data were performed through the phase tensor method to investigate the general geometry of the sought reservoir for running a 2D TE + TM mode inversion scheme. Through 2D inversion of the MT data along three profiles across the favorable zones, the electrical resistivity models were used to image sedimentary units (i.e., cap rock, top soil, bedrock and reservoir) and magmatic rocks. Considering both geophysical properties led to illustrate a plausible geothermal reservoir in the area.

INTRODUCTION

Iran is a favorable region in terms of high geothermal potential due to its intimate link to tectonic activities and occurrence of large volcanic belts. Figure 1 indicates the volcanic belts and the distribution map of geothermal potential areas in Iran. The Mahallat region is one of the recognized geothermal fields in Iran, and several studies have been recently dedicated to investigate its potential

for trapping geothermal reservoirs (e.g., Oskooi and Darijani 2014; Mohammadzadeh Moghaddam et al. 2016). The vast expanse of Mahallat and lack of exploratory information have made it difficult to evaluate precisely its geothermal favorability. However, the presence of hot springs within the Abgarm range has created a special exploratory indicator for the region. The name "Abgarm" in Persian means "hot water," which indicates the originality and famousness of the hot springs in the region. The area surrounding the hot springs in Abgarm contains young volcanic rocks, altered units, extensive travertine outcrops and intrusive bodies, which are considered important key factors of potential geothermal fields. Hence, the hot springs in Abgarm have motivated geophysicists to

[1]Institute of Geophysics, University of Tehran, Tehran, Iran.
[2]School of Mining Engineering, College of Engineering, University of Tehran, Tehran, Iran.
[3]To whom correspondence should be addressed; e-mail: maysamabedi@ut.ac.ir
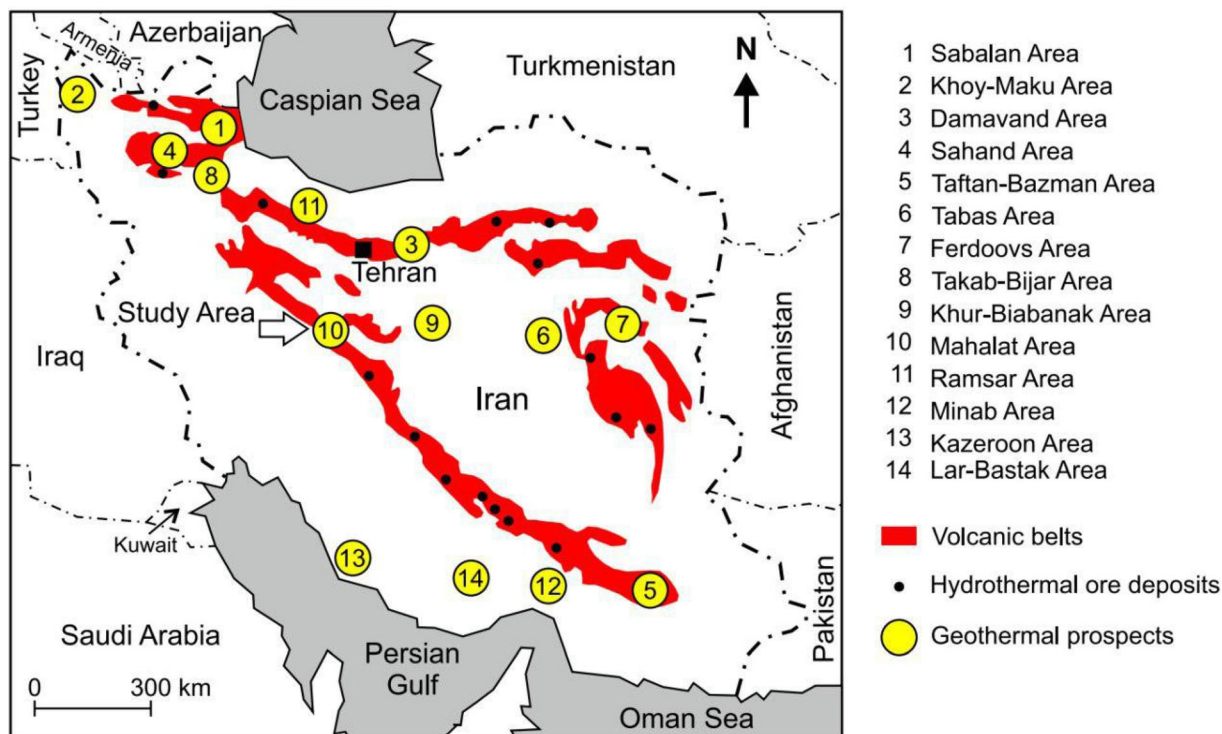
Figure 1. Distribution of geothermal prospects in Iran (Renewable Energy Organization of Iran, SUNA 1998; Noorollahi et al. 1998; Yousefi et al. 2010).

conduct magnetometric and magnetotelluric (MT) geophysical surveys in view of that geological evidence.

Prior studies in the region state that the heat of hot springs is due to the cooling process of subsurface molten magma. Rezaie et al. (2009) presented a conceptual model on formation of the hot springs in the region. According to their model, rainfall and meteoric waters mixed with magmatic fluids charge the hot springs and infiltrate into the earth through transverse faults, fractures and permeable units. By addition of high pressure vapors and other volatiles (i.e., H_2O, CO_2, H_2S) originating from magma body or other high-temperature rocks in depth, the infiltrated waters become more soluble. The density of the infiltrated waters decreases because of increase in temperature at depth and in proximity to the cooling magma feeder or the surrounding hot rocks capturing the volatiles. Consequently, they become more buoyant and rise up along faults. During the rising and reacting with the surrounding carbonate rocks, the temperature decreases and more volatiles dissolve in the water. Therefore, the solubility of hot waters increases through the formation of deep karst

networks. The mixing of hot waters with shallow cool waters also affects the dissolution of carbonate rocks. The ascent of waters to shallower levels and depletion of hydrostatic pressure causes the release of gases (e.g., CO_2) as well as the formation of saturated waters with carbonate calcium (calcite). Deposition of carbonate calcium leads to the formation of travertine surrounding hot springs (e.g., Beitollahi 1996; Rezaie et al. 2009; Oskooi et al. 2013). Geochemistry and hydrology researches indicated that the average temperature of the hot springs in Abgarm is 45 °C with pH ranging from acidic to neutral (Rezaie et al. 2009; Yazdi et al. 2016). Geothermometric studies on the Mahallat reservoir also revealed that the approximate temperature was estimated to range from 88 to 194 °C (Nouraliee and Ebrahimi 2012). Geological and geochemical studies indicated that the hydrothermal fluid cycle in the region was controlled mainly by N–S trending faults (Porkhial et al. 2013). Yazdi et al. (2016) reported, based on hydrogeochemical analysis of samples, a low concentration of heavy metals in fluids and the least harmful effects for the environment. In addition, low changes in discharge of

hot springs, their temperature, and high partial pressure of CO_2, have led to the conclusion that the hot springs were located on faults and had deep aquifers. Rezaei et al. (2018) stated that the geothermal system is associated with a deep fault zone and can be categorized as a convection dominated geothermal system. In fact, the local rainfall over the adjacent highlands percolates into the ground along the main active fault in the region and then heats up and emerges finally at the lowest topographic elevation of the fault in the form of hot springs characterized by temperature ranging from 30 to 52 °C. Water samples from the hot springs have high electrical conductivity values (ranging from 6585 to 11,265 μS/cm) with chloride water type. Rezaei et al. (2018) declared that the lower circulation depth of meteoric water in the geothermal system was about 3000 m by considering the possible maximum geothermal gradient of about 46 °C/km, which is also in line with our findings and proposed geological model. They concluded that the hydrothermal fluids mix predominantly with shallow cold groundwater during their ascent, and the proportion of cold shallow and deep-hot water was about 70% and 30%, respectively (Yazdi et al. 2016; Rezaei et al. 2018).

Having applied 2D inversion on a single MT profile using the Occam approach, Oskooi et al. (2013) stated that the geothermal reservoir is located within 500–2000 m and the heat source depth starts from 1000 m depth. Benefiting from 2D inversion of MT data through MT2DInvMATLAB code along two perpendicular profiles, Oskooi et al. (2013) declared that the fluid reservoir is resolved at depths of 1000–3000 m and the geothermal resource is located at about 7000 m or deeper. Through Euler and An-Eul depth estimation (i.e., an analytic signal and Euler deconvolution approach) using ground magnetometry data and the 2D Occam inversion methodology on a single profile of MT data, Oskooi and Darijani (2014) performed an integrated interpretation, proposed a geological model and concluded that the reservoir exists within depths of 800–2000 m and the heat source extended from 1000 m to greater depths. Nouraliee et al. (2015) used 3D gravity inversion, Euler's depth estimation and horizontal gradient maps to study the density contrasts and complex fault system of the region, and they stated that the subsurface rocks within depths of 1000–3000 m are the most suitable aquifers for utilization of geothermal energy. From these mentioned previous researches, no geological model has been proposed according to multiple geophysical datasets. Besides, there are some differences on the concluded depth estimates in the previous researches.

Deploying various geophysical methods helps to suppress intrinsic ambiguity arising from data interpretation. However, because hydrothermal activities have drastic impact on electrical resistivity and magnetic susceptibility of host rocks, utilization of magnetometry and MT techniques can be of great contribution in studying subsurface structures of geothermal targets (Oskooi et al. 2005; Spichak and Manzella 2009; Bruhn et al. 2010; Peng et al. 2019). Generally, in geothermal zones, the presence of igneous rocks with abundant magnetic minerals enhances the efficiency of the magnetometry method in exploring for intrusive bodies (Abdel Zaher et al. 2018). In addition, frequent application of magnetometry in identifying faults and demagnetized zones is an important factor in the practicality of magnetometry method in geothermal areas (Paoletti et al. 2009). Geothermal sources are favorable targets for electromagnetic methods due to formation of strong variations in electrical resistivity of subsurface rocks. Among the different electromagnetic methods, MT has been an impactful procedure in the investigation of deep geological structures. The MT method has also been widely used in geothermal studies (e.g., Johnston et al. 1992; Mogi and Nakama 1993; Munoz 2014; Amatyakul et al. 2015; Patro 2017).

In this study, the interpretations and the presented geological model were based on both magnetometry and MT inversion models in order to obtain a more accurate model with less depth ambiguity. In addition, three parallel MT profiles covered more lateral distance compared to one or two intersecting profiles. The three profiles of MT data were modeled in 2D using the nonlinear conjugate gradient (NLCG) method (Rodi and Mackie 2001). The magnetometry data were also modeled in 3D through the Li–Oldenburg method (Li and Oldenburg 1996). The depth of magnetic sources was also estimated by Euler's procedure to achieve a general view about the depth of shallower intrusive bodies (Reid et al. 1990; Ravat 1996). Finally, a plausible geological model was inferred from simultaneous consideration of geophysical models and geological evidence, which facilitate imaging of the geothermal mechanism of the study area. According to geological and geophysical information, the results seem promising for further explo-
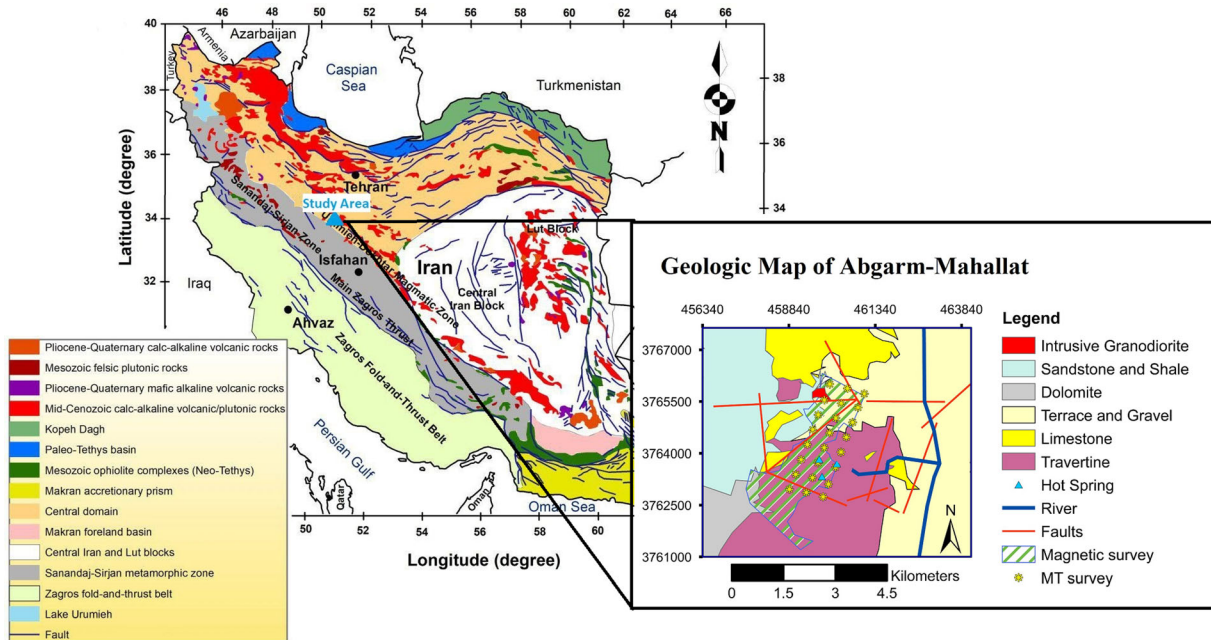
Figure 2. Geological map of the Abgarm-Mahallat area over Iran's structural geological map (reproduced with permission from Richards et al. 2006). The inset presents the detailed geological setting of the studied area. The magnetometry and MT surveys are superimposed on the map (reproduced from the archive of the Geological Survey of Iran, GSI).

ration and drilling because no wells have been drilled in the Abgarm geothermal region so far. Berktold (1983) reported a basic conceptual model indicating the main components of similar type of geothermal system as well.

GEOLOGICAL SETTING OF ABGARM OF MAHALLAT

Located in the volcanic zone of Central Iran, the Mahallat region is situated in the middle of the country. The old zone of Central Iran has been active and energetic during different geological periods. The west side of the Central Iran is bounded by the Sanandaj–Sirjan metamorphic zone (SSZ). The north side is bounded by Alborz zone, while the southern part is enclosed by the Makran zone. In terms of permeability aspect, the Central Iran zone is highly permeable considering the expansion of calcareous and dolomite units and the presence of cracks and joints. Geological structures in this region are characterized by dextral rotational movement formed by northward under-thrusting of the Arabian Plate beneath the Iranian Plate (McKenzie 1972; Jackson et al. 2002; Ritz et al. 2006). Considering this tectonic framework, the Cenozoic geologic

history and the stratigraphy of this region are complex and, as a result, the stratigraphic record of the area is made up of units with different structural characteristics. During Eocene, igneous activities took place in this region and caused accumulation of volcanic rocks over the Mesozoic and Paleozoic sedimentary strata. Subsequently, these rocks were thermally metamorphosed by an early Miocene monzonitic batholith, which is elongated in a NW–SE direction. Tectonic movements over the past geological periods have caused faults in and around the rock units of the region. Generally, faults of the region have two main directions, NW–SE and NE–SW. The most prominent fault of the region is the Mahallat–Abgarm fault with nearly N–S direction around the Abgarm area. All hot springs in the region are strongly connected to tectonic activities and this active fault zone. The length of the mentioned fault is about 50 km. Small-scale faults are also observed at the boundary of the formation units, which appear to be some splits of the mentioned fault. Figure 2 depicts the geological map of the Abgarm area in the structural geology map of Iran accompanied with its simple geological setting. The area is covered by a sedimentary package ranging from Permian to Quaternary in terms of age. The outcropping formations within the study area in-

clude the Shemshak Formation (with lithology of Jurassic shale and limestone), Lar Formation (with lithology of Cretaceous Orbitolina bearing limestones), Qom Formation of Miocene age (with lithology of marly limestones) and igneous rocks of granodiorite are exposed in the vicinity of such sedimentary units.

The hot springs at Abgarm, whose locations are indicated on the geological map (inset map in Fig. 2), flow from travertine and alluvial sediments. Established over time by sediment deposition of hot springs, the travertine sediments were formed adjacent to faults in the area and have an approximate thickness of 500 m. These springs are faulted with maximum discharge of 42 to 45. Minor fluctuations in discharge and temperature in the Abgarm hot springs and their high partial pressure of CO_2 in aquifers are some signs of deep-hot springs (Oskooi et al. 2016; Yazdi et al. 2016). The hot springs are rich limestone minerals, leading to deposition of thick travertine sediments around the craters of the springs. Faults and fractures have important impact on the circulation of water from the surface down to deeper levels. Another remarkable point is the abundance of alterations in the study area. Most of the alterations in the area are argillization–sericitization, while kaolinitization–alunitization alterations are sporadic in the area. These types of alterations, especially the former, are closely related to the activity of hydrothermal fluids and occur mainly at high temperatures (Oskooi et al. 2013; Oskooi and Darijani 2014; Oskooi et al. 2016).
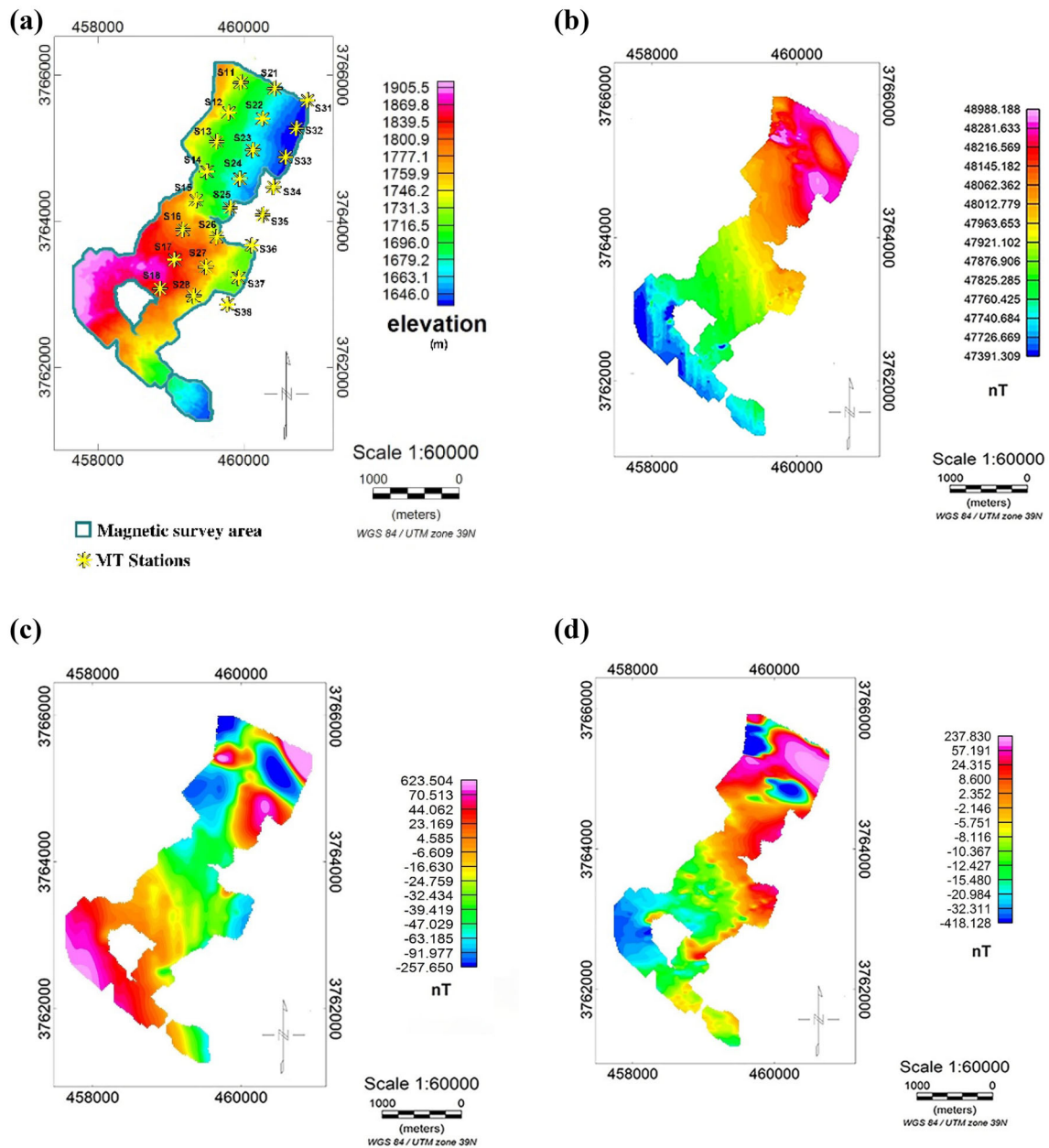
MAGNETOMETRY SURVEY

As illustrated in Figure 2, a magnetometry survey with over 10,000 data points was conducted around the hot springs. The direction of magnetic survey was almost from SW toward the NE. The approximate data point interval was 1 to 5 m, and some data points were taken more than once for double check. Some low-quality and noisy data were removed and interpolated in the dataset to improve data precision and quality. The dimensions of the magnetic survey area were 4660×2600 m^2. This area is indicated with green hatches relative to MT stations and geological units in Figure 2. However, the study area had a severe topography, and the steep slopes of the ground caused an irregular shape of the magnetic grids and an irregular distribution of magnetic data. Figure 3a indicates the topography

over the magnetic survey area and the MT stations located in the Abgarm area, where the difference between the northeast and southwest elevations of the area was 259 m. Figure 4b indicates the total magnetic field intensity in the Abgarm area. After de-trending the regional Earth's magnetic field using a first degree removal of polynomial trend (Beltrão et al. 1991; Thurston and Brows 1992), the magnetic residual map was obtained (Fig. 3c). On the residual map, an anomaly of +623 nT is evident at the northeastern parts.

Reduced-to-pole (RTP) filter is a prevalent tool in magnetometry studies; it facilitates the interpretation of sophisticated multi-source anomalies. It converts magnetic signals to a symmetrical pattern, meaning that magnetic data are only induced with the vertical component of the Earth's magnetic field. Note that the RTP map eliminates the dipolar nature of magnetic anomalies, converts their asymmetric signal to a symmetric one, and shifts anomaly peaks over the main causative sources (Abedi and Oskooi 2015). To simplify interpretations and to obtain better understanding of the magnetic anomaly, the RTP filter was applied to the data and a clear anomaly appeared at the northeastern corner of the grid (Fig. 3d).

To obtain a basement depth from the anomaly, the standard Euler's deconvolution was used (Reid et al. 1990; Ravat 1996). In this approach, the Euler differential equation is solved for the entire gird, while a directional derivative of the magnetometry data is considered as input to run the depth estimator. The Euler method is dependent on the shape of the body, which enters into the differential equation as the structural index (SI). To achieve a proper estimation of SI, we calculated several structural indices by trial and error from SI = 0 to SI = 3 with 0.1 increase in each single step to obtain a more precise estimate. According to the existing geological information, previous studies of the area, and the geological map and reports of this area, there exists an intrusive magmatic body at depth. Oskooi et al. (2016) declared that the SI is between 1 and 2 and the anomaly shape is between a dyke and a vertical cylinder. Considering this fact, we started Euler estimations with several SI values and window sizes. The best results with acceptable clustering and regularity were achieved for SI = 1, and the results (depth estimations with the optimum SI = 1) were also in line with the sections of the 3D magnetic model along with the results of previously conducted studies. The following criteria were used to dis-

Figure 3. Measured magnetometry data over the Abgarm geothermal prospect zone. (**a**) Elevations. (**b**) Total magnetic field intensity. (**c**) Residual magnetic data after de-trending the regional EarthGúøs magnetic field effect. (**d**) Reduced-to-pole data.

criminate between the calculated solutions, after Beiki (2010):

1. Estimated source locations with standard deviations to the estimated depth ratio greater than a predefined threshold were rejected.

2. Only solutions with horizontal coordinates located within the window were accepted.
3. Solutions with estimated depths greater than a predefined threshold are rejected. (Thompson 1982; Beiki 2010; Mohammadzadeh-Moghaddam et al. 2012; Oskooi et al. 2016).
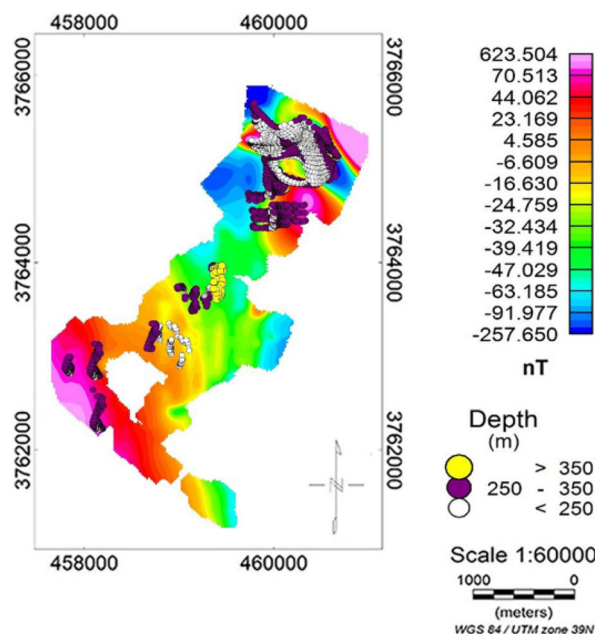
**Figure 4.** Euler depth estimation for SI = 1.

Considering the range and dimensions of the body, a window of 400×400 m^2 was assumed for the depth estimation process. This yielded proper results, which could fit the anomaly scope appropriately. In addition, according to the sill-like shape of the shallow bodies from geological evidence, the SI was set to 1 to estimate the top depth of the shallow magmatic units.

Three depth intervals were assumed in order to plot the estimates. In Figure 4, the white circles depict depths of 250 m and below, the purple circles represent depths of 250 to 350 m, and the yellow circles represent depths greater than 350 m. The estimates of lower depths can indicate surface alterations of the sedimentary rocks in the area. Based on these depth estimates, a basement depth of 250 to 350 m was predicted for the subsurface magnetic body that has apparently risen to shallow depths and given its heat to the surrounding spring water and rocks. This shallower anomaly is possibly a branch of a deeper magmatic source, which is still cooling and acting as a heat source of the system.

To invert the ground magnetometry data of the Abgarm, the Li–Oldenburg inversion algorithm was utilized. For this, three required input files of the observed data, 3D mesh, and topography data were prepared. A noteworthy point is that, considering the general grid figure of the data and the NE–W

elongation of the survey area, to expedite and simplify the 3D inversion process of the data, the data were rotated 60° clockwise to make an E–W figure and to avoid additional meshes that may slow down the modeling process speed (Fig. 5a). This action practically added 60° to the magnetic declination angle but did not affect the magnetic inclination angle. Due to trivial misfit between the observed and calculated data from the inversion algorithm, the conducted inversion was acceptable (Fig. 5b).

To have a better display of the body, the depth 2000 m was used in this image. It should be mentioned that this model is viewed for a susceptibility cutoff value of 0.05 SI. Based on the magnetic susceptibility model (Fig. 5c), a magmatic body with relatively high magnetic properties due to formation of magnetic minerals has risen up to low depths. Because there are some hot springs placed on wet sedimentary units on the surface down to low depths, the up-risen high temperature magma started the process of transferring its heat to the surrounding water and sedimentary units. This led to a gradual decrease in magma temperature to lower degrees than the Curie point resulting in the crystallization of magnetic minerals according to Bowen reaction series (Yoder 2015). The position of the hot springs relative to the intrusive magmatic body and
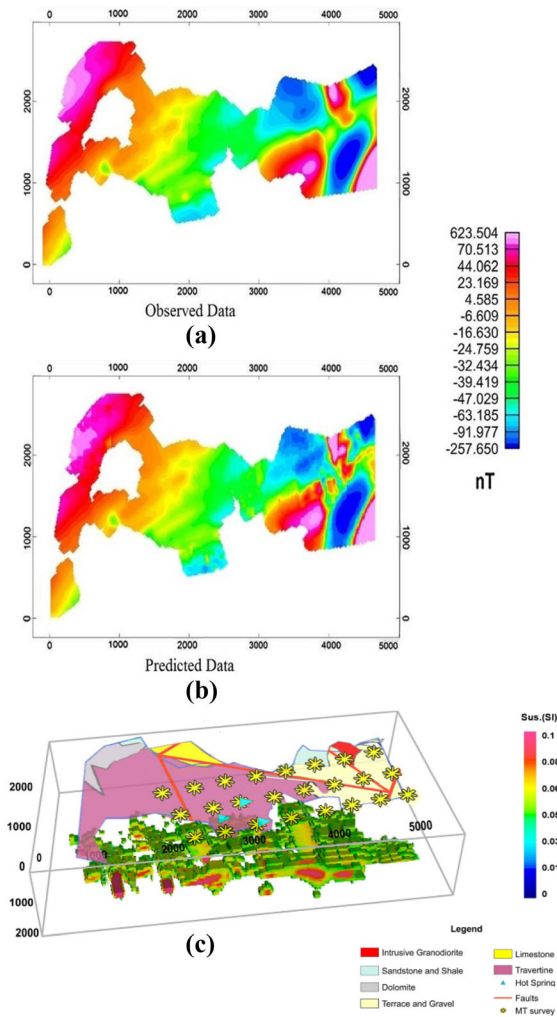
Figure 5. (a) Observed magnetometry data and (b) predicted data for (c) an inverted model overlaid on the survey area with geological units and positions of hot springs. The 3D volume rendering view of the magnetic susceptibility model is shown for a cutoff value of 0.05 SI.

the variations in susceptibility and resistivity sections are shown in Figures 9, 10 and 11. This uprisen intrusive body can be a split of a deeper magmatic mass, which seems to be a proper heat source for the hot springs. The achieved basement depth of the 3D inversion was also in good agreement with the depth obtained by the Euler method.

MAGNETOTELLURIC SURVEY

To obtain electrical resistivity changes in subsurface structures in the study area, a MT survey was conducted along three parallel profiles, which are

marked with yellow asterisks in Figures 2 and 3a. It should be noted that these profiles were also the locations of the magnetic 2D inversion sections. Each profile consisted of eight stations with approximate distance of 500 m. The direction of the profiles was NE to SW. The periodic interval of the data among various sites ranged mostly from 0.01 to 14 s. The D + criterion was beneficial in smoothing the curves. To depict a schematic of the MT data quality, the apparent resistivity and phase of a few characteristic sites (example sites) presented in Figure 6 also contain the fittings, showing a relatively acceptable condition of the survey and inversion. Prior to modeling, to specify the dimensionality and the dominant strike of the subsurface structures in the study area, the phase tensor method was applied because it is not affected by non-inductive distortions (Caldwell et al. 2004). In this method, if the skew angle (β) is statistically within -5 to 5, a 2D strike can be considered for subsurface structures.

In Figure 7, the horizontal and vertical axes represent the skew angles in degrees and the number of data points, respectively. Because most of the skew angles in data points are within -5 to 5 degrees along each profile, the 2D inversion of the MT data can be justified, while there exist some 3D effects in the area. In the phase tensor method, the $\alpha - \beta$ values return the strike of the structures. Rose diagrams were plotted to represent the obtained strikes (Fig. 8). The estimated directions have 90° ambiguity of geoelectric strike in the MT method. Despite the presence of relative scatterings, especially for the third profile, the distribution of directional values makes it possible to select a dominant direction. The geological information, such as the N–S trend of the Mahallat active fault in the region together with the previous studies in the region, made it possible to select the N26W azimuth as the final direction of the geoelectric strike within the study area in order to perform a 2D inversion.

For the inversion of the MT data of Abgarm, the NLCG method was implemented for TE + TM modes (TE: transverse electric, and TM: transverse magnetic). After designing an appropriate mesh for the models, some different models with various parameters were tested to obtain the most accurate model. Hence, diverse initial models were examined. The inversion process was performed using initial resistivity values of 10, 100 and 1000 O-meter, while no significant difference was observed in terms of root-mean-square (RMS) decrease and the conver-
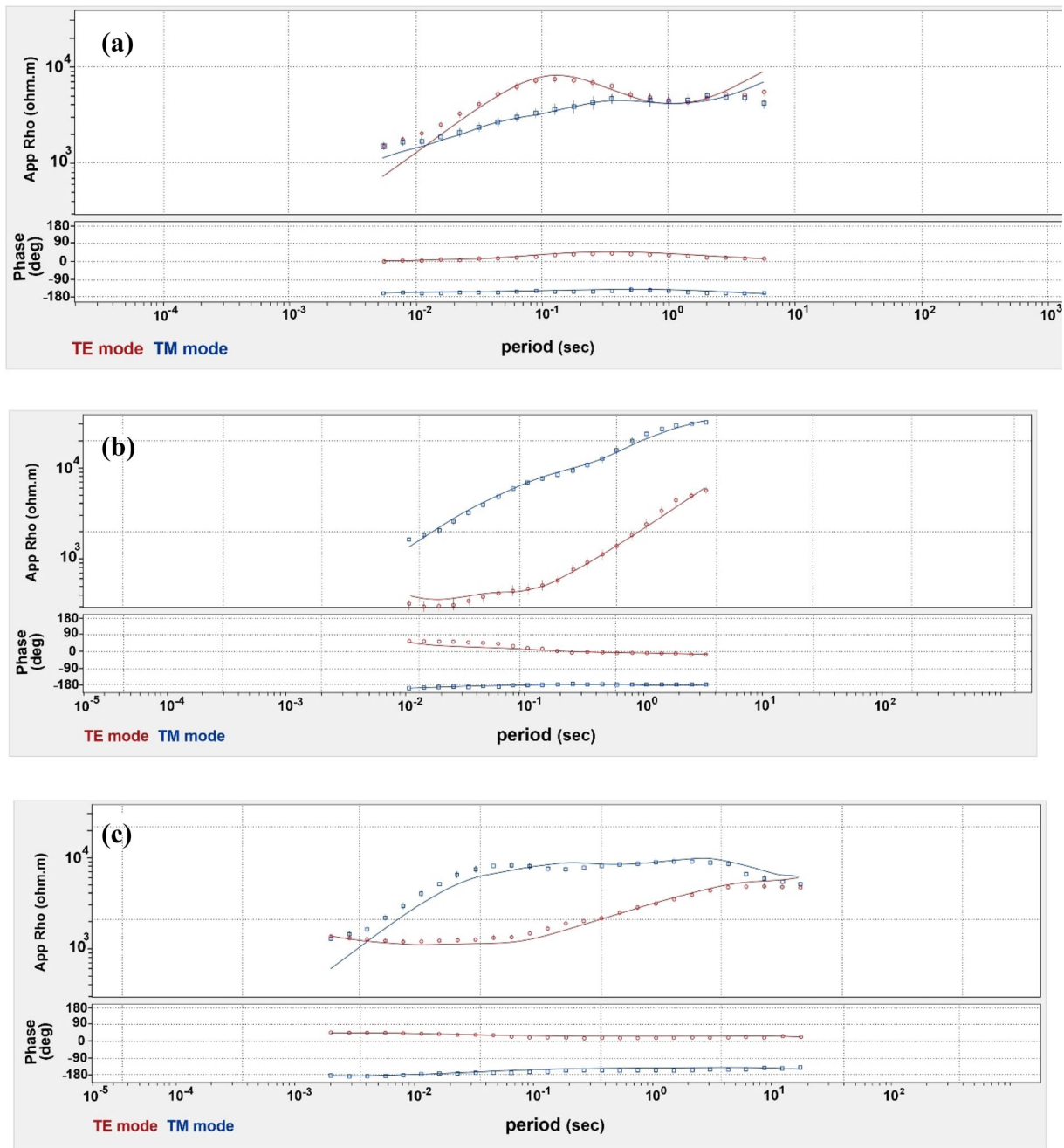
Figure 6. Characteristic sites presenting apparent resistivity and phases of TE & TM modes, along with data fittings from each 3 MT profiles including (a) the station number 2 from the first profile (S12), (b) station number 6 from the second profile (S26), and (c) station number 3 from the third profile (S33).

gence process. Because increasing the error floor value causes decrease in RMS, the error floor of 20% for the apparent resistivity and 5% for phase values were assumed through definition of various error floor values by trial-and-error. The inversion process was performed for different tradeoff (τ)

parameters to decrease the RMS values. Therefore, the best results were achieved for $\tau = 1$, which is a common approach for datasets with high RMS due to several reasons. In addition to prioritizing the phase values by allocating lower error floors than those of resistivity, static shift corrections were also
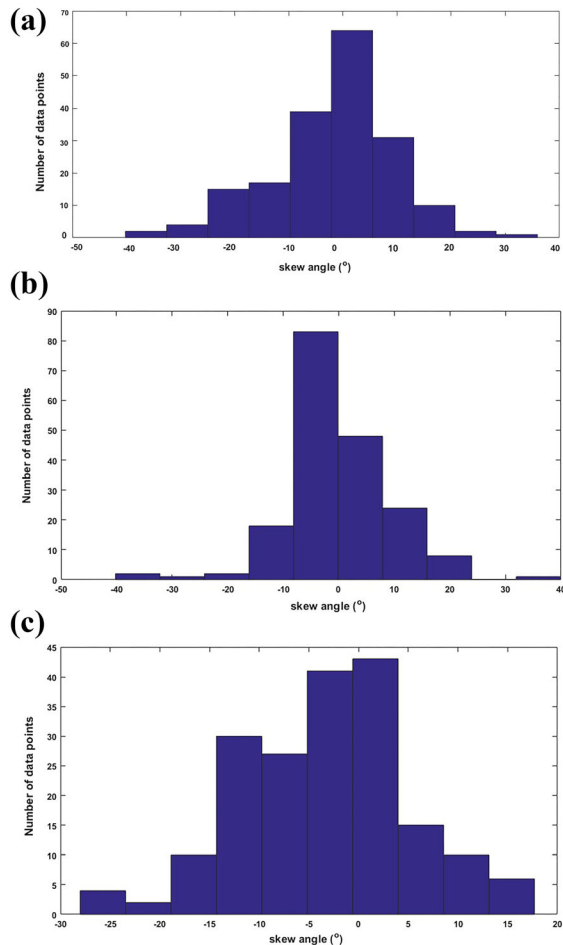
Figure 7. Histogram plots of skew angles along profiles (a) 1, (b) 2, and (c) 3.

made prior to inversion process, which also made drastic changes in reduction in RMS values. In advance of presenting 2D models of data inversion, the pseudo-sections of apparent resistivity and phase in TE and TM modes were investigated for each profile (Figs. S1-S6 provided in the Supplementary Information). In line with the presented pseudo-sections (Figs. S1-S6 provided in Supplementary Information), it can be stated that the 2D inversion process possesses a proper misfit.

INTEGRATED INTERPRETATIONS

For beneficial comparison of the results of the 3D inversion of magnetometry and the 2D inversion of MT data, three vertical slices were extracted from the 3D magnetic susceptibility model below the

magnetotelluric profiles to make an integrated interpretation (Figs. 9, 10, 11). In the MT section of the first profile (Fig. 9a), it can be seen that due to the presence of the hot springs together with the wet sedimentary units and the associated alteration, significantly low resistivity structures were formed at shallow depths. From 250 to 1500 m depth, the resistivity of the subsurface rocks also increased and, in deeper areas, it decreased again. The reduction in resistivity values at high depths (2–4 km) can indicate the heat source of the system. In the magnetic section of the first profile (Fig. 9b), the rocks have high magnetic susceptibility resulting in high magnetism within depths of 250 to 1500 m. This occurrence indicates an intrusive granodiorite body that has risen and lost its temperature while being cooled through a wet sedimentary environment. As the magmatic intrusive mass cools, according to the famous Bowen's reaction series, a harder crystallized unit is formed with greater susceptibility and resistivity than the host wet sedimentary units. It seems that the high temperature of the hot springs can be due to the cooling process of the intrusive bodies. It is worth noting that the depth from the obtained inverse model was compliant with the Euler deconvolution estimation, which confirms the accuracy of the modeling procedure.

In terms of geographical location in the middle of the study area and the presence of hot springs, the second profile may have a special importance. It is worth noting that previous studies have also been conducted on this profile in terms of the location of the presented geological model (Oskooi and Darijani 2013; Oskooi et al. 2013, 2016). The existing hot springs between stations 25 and 26 have increased the conductivity of the surrounding shallow rocks (Fig. 10a). On the right-hand side of the MT section, there is a high resistivity body with high magnetic susceptibility values in the magnetic section; it may represent an intrusive body that altered the surrounding rocks. In the lower and middle part of the magnetic section at depths of 2–4 km, a body with relatively high magnetic susceptibility is evident (Fig. 10b). The lower susceptibility values of this body compared to the shallow one can be due to its higher temperature that led to less crystallization and magnetic minerals. It may also be possible that the wetness of this deeper body compared to the shallow one has caused the same resistivity range with the surrounding rocks preventing from appearing in the MT section. In the magnetic section, the two semi-vertical traces beside the deeper
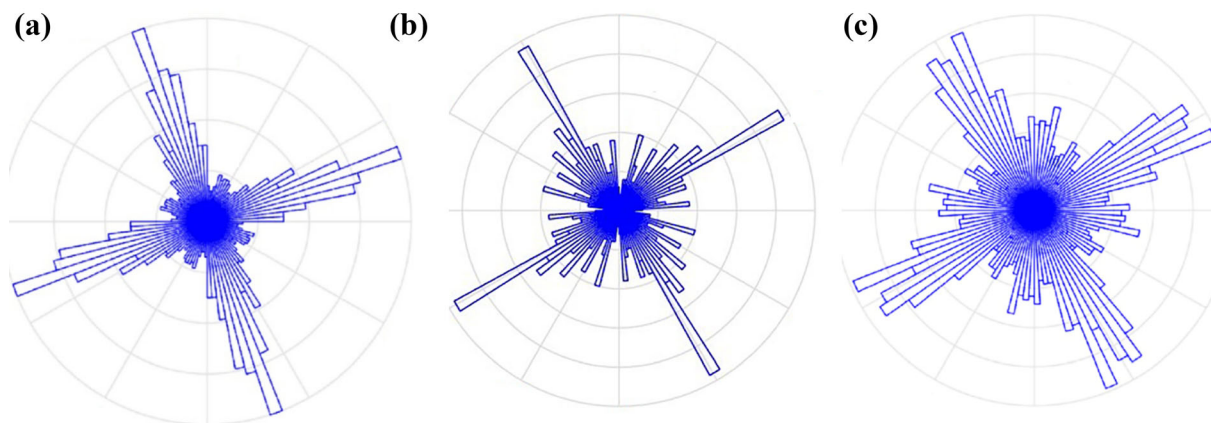
Figure 8. Rose diagrams of geoelectric strikes for (a) profile 1, (b) profile 2, and (c) profile 3.
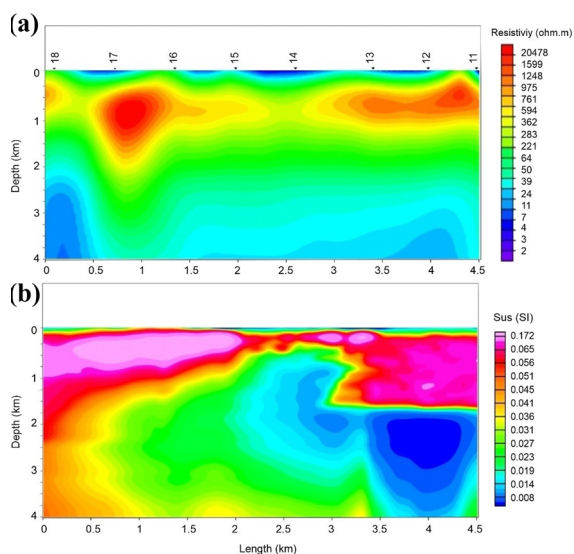

Figure 9. (a) Electrical resistivity and (b) magnetic susceptibility models across profile 1, where a 2D TE + TM mode inversion was run for MT data accompanied with a 3D inversion algorithm for magnetometry data.
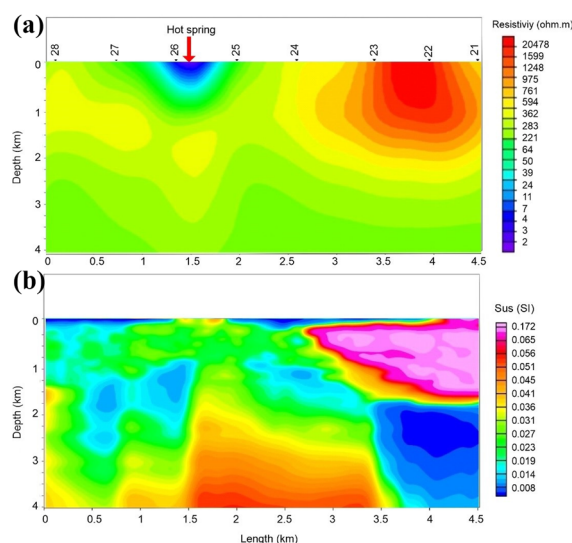

Figure 10. (a) Electrical resistivity and (b) magnetic susceptibility models across profile 2, where a 2D TE + TM mode inversion was run for MT data accompanied with a 3D inversion algorithm for magnetometry data.

body (interpreted as the heat source) can be two major hidden faults of the area that have a very prominent role in the circulation of spring water to deep levels. The three pale blue decreases in the middle of the section can be also recognized as the hidden minor faults playing important role of fluid movement and circulation to the reservoir.

Similar to the previous profiles, an intrusive granodiorite body, with higher resistivity and susceptibility than the host rocks, is extended across profile 3 (Fig. 11a). In all three profiles, this intrusive body is stretched from shallow depths of 250 m to

1000-1500 m around the hot spring, and a high conductivity part is evident between stations 35 and 37. The blue boundary in the middle of the magnetic section (also attributed to minor faults in the second profile section) could be related to a minor fault (Fig. 11b). On the left-hand side of the magnetic section, the intrusive body elongation continues up to the depth 4 km (the depth of heat source), which illustrates the magma intrusion path from the heat source up to a sill-shaped body (250 m to 1500 m) that also altered the surrounding rocks.
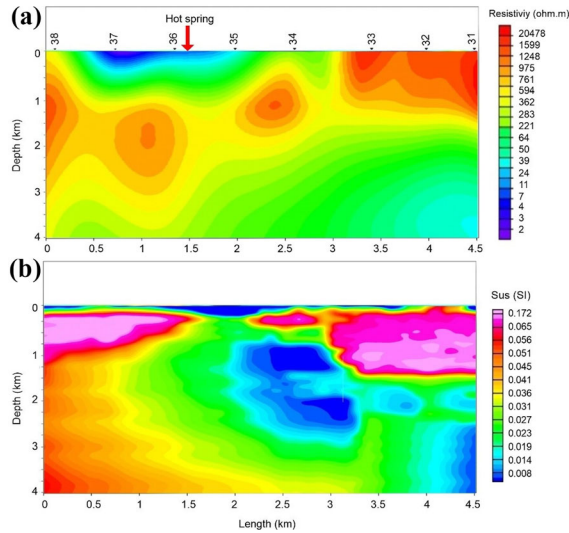
Figure 11. (a) Electrical resistivity and (b) magnetic susceptibility models across profile 3, where a 2D TE + TM mode inversion was run for MT data accompanied with a 3D inversion algorithm for magnetometry data.

RESERVOIR CONFIGURATION

After performing the inversion step, based on the physical properties and the geological information, a plausible geological model was proposed for investigating the material and changes of subsurface features along with the geothermal system mechanism (Fig. 12). As illustrated, the layers of the area include travertine (cap rock) down to 250 m, young terraces (top soil) down to 250 m, sandstone and shale (reservoir) starting from 250 m down to 2.5 km, granodiorite lava (cooled acidic intrusive body) from 250 down to 1.5 km, limestone (bedrock) from 1.5 to 4 km, and a probable cooling volcanic body (heat source) within the depths of 3 to 4 km probably down to deeper levels. According to the geothermal reservoir model, the major hidden faults of the area play an important role in the movement and circulation of fluids. Limestones and carbonate rocks can be proper bedrocks due to high porosity and low permeability. Sandstones with interbedded compositions of shale have high porosity and permeability and can be suitable reservoirs. The intrusive body on the right-hand side of the model is a granodiorite that has cooled during time. It is worth noting that this intrusive unit was interpreted as mafic and ultra-mafic rocks in previous studies (Oskooi et al. 2016), and this study
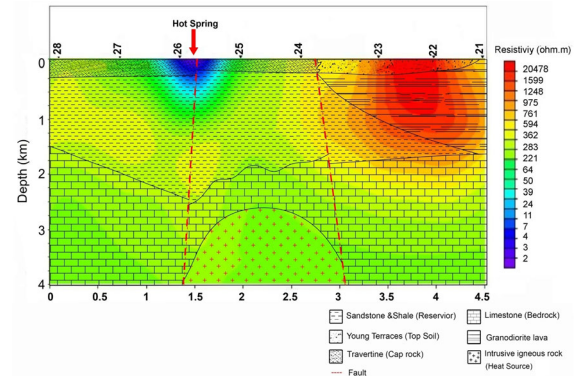
Figure 12. A geologically plausible geothermal reservoir in the Abgarm area inferred from simultaneous consideration of geophysical models (electrical resistivity and magnetic susceptibility) and geological evidence overlaid with resistivity changes.

renewed and updated a more precise interpretation of the nature of this igneous intrusion according to geological and geophysical assessments (Aghanabati 2004). At the northern portions of the geological map of the study area, there exists a granodiorite unit; this is the reason for interpretation of the granodiorite material. Spring and meteoric fluids penetrate deeper through the faults and pores and return to the surface as temperature rises around the cooling intrusive magma. The lower folds of the sandstone unit or the reservoir are related to the pressure caused by the magma intrusion beneath the reservoir.

CONCLUSIONS

The Abgarm area of the Mahallat region, located in the large volcanic belt of Iran, is one of the areas with top potential for geothermal energy utilization. To probe into the geothermal mechanism of the subsurface structures, magnetotelluric and ground magnetometry methodologies were exploited. Through Euler depth estimation from the magnetic data, a basement depth range of 250–350 m was calculated for shallower magnetic features that have risen up and cooled, transferring the heat to the surrounding rocks and the reservoir. The shallow intrusion is likely a split branch of a deeper magmatic intrusion, which is still cooling. To obtain better understanding of the subsurface changes in magnetic susceptibility, 3D inversion of the mag-

netic data was performed. Dimensionality analysis and strike estimation were also implemented on three profiles of the MT data. The data were then rotated westward to achieve the actual TE and TM modes data. Then, a 2D inversion was run on the data using the nonlinear conjugate gradient method. To make a desirable comparison between the 3D magnetic susceptibility model and the 2D electrical resistivity model, three vertical sections were extracted from the 3D susceptibility model right beneath the MT profiles. According to the three achieved magnetic susceptibility and resistivity pair sections and the geological information of the study area, a geological model was proposed to express and visualize the geothermal mechanism of the region. Accordingly, the units of travertine, young terraces, sandstone and shale and limestone were determined as cap rocks, top soil, reservoir and bed rock at the depth ranges of 0–250 m and 250 m to 2.5 km and 1.5–4 km, respectively. Revealed by Euler depth estimation and 3D magnetic inversion, a granodiorite lava intrusion was also specified within depths of 250 m to 1.5 km. Based on the geological map, this unit also outcrops at the northern part of the study area. At deeper levels, a cooling volcanic body is interpreted as the heat source of the system at depth range of 3–4 km, probably extending to deeper levels. This cooling magmatic body heats up meteoric waters descending through the faults and fractures. The heated water becomes buoyant and loses density. Therefore, it rises up through the faults and fractures and forms a hot spring on the surface.

ACKNOWLEDGMENTS

ELECTRONIC SUPPLEMENTARY MATERIAL

The online version of this article (https://doi.org/10.1007/s11053-020-09739-8) contains supplementary material, which is available to authorized users.

REFERENCES

Abdel Zaher, M., Saibi, H., Mansour, K., Khalil, A., & Soliman, M. (2018). Geothermal exploration using airborne gravity and magnetic data at Siwa Oasis, Western Desert, Egypt. *Renewable and Sustainable Energy Reviews, 82,* 3824–3832.

Abedi, M., & Oskooi, B. (2015). A combined magnetometry and gravity study across Zagros orogeny in Iran. *Tectonophysics, 664,* 164–175.

Aghanabati, A. (2004). *Geology of Iran*. Tehran: Geological Survey of Iran.

Amatyakul, P., Rung-Arunwan, T., & Siripunvaraporn, W. (2015). A pilot magnetotelluric survey for geothermal exploration in Mae Chan region, northern Thailand. *Geothermics, 55,* 31–38.

Beiki, M. (2010). Analytic signals of gravity gradient tensor and their application to estimate source location. *Geophysics, 75*(6), I59–I74.

Beitollahi, A. (1996). *Travertine formation and the origin of the high natural radioactivity in the Region of Mahallat hot spring*s. M.Sc. Thesis. Islamic Azad University of Tehran, Iran, 120 pp.

Beltrão, J. F., Silva, J. B. C., & Costa, J. C. (1991). Robust polynomial fitting method for regional gravity estimation. *Geophysics, 56*(1), 80–89.

Berktold, A. (1983). Electromagnetic studies in geothermal regions. *Geophys Surv., 6,* 173–200.

Bruhn, D., Manzella, A., Vuataz, F., Faulds, J., Moeck, I., & Erbas, K. (2010). Exploration methods. In E. Huenges (Ed.), *Geothermal energy systems* (pp. 37–112). Wiley.

Caldwell, T., Bibby, H., & Brown, C. (2004). the magnetotelluric phase tensor. *Geophysical Journal International, 158,* 457–469.

Jackson, J., Priestley, K., Allen, M., & Berberian, M. (2002). Active tectonics of the South Caspian Basin. *Geophysical Journal International, 148,* 214–245.

Johnston, J. M., Pellerin, L., & Hohmann, G. W. (1992). Evaluation of electromagnetic methods for geothermal reservoir detection. *Geothermal Resources Council - Transactions, 16,* 241–245.

Li, Y., & Oldenburg, D. W. (1996). 3-D inversion of magnetic data. *Geophysics, 61*(2), 394–408.

McKenzie, D. S. (1972). Active tectonics of the Mediterranean region. *Geophysical Journal of the Royal Astronomical Society, 30,* 109–185.

Mogi, T., & Nakama, S. (1993). Magnetotelluric interpretation of the geothermal system of the Kuju volcano, southwest Japan. *Journal of Volcanology and Geothermal Research, 56,* 297–308.

Mohammadzadeh Moghaddam, M., Mirzaei, S., Nouraliee, J., & Porkhial, S. (2016). Integrated magnetic and gravity surveys for geothermal exploration in Central Iran. *Arabian Journal of Geosciences, 9,* 506.

Mohammadzadeh-Moghaddam, M., Oskooi, B., Mirzaei, M., & Jouneghani, S. J. (2012). Magnetic studies for geothermal exploration in Mahallat, Iran. In *Istanbul 2012-international geophysical conference and oil and gas exhibition* (pp. 1–4).

Society of Exploration Geophysicists and the Chamber of Geophysical Engineers of Turkey.

Munoz, G. (2014). Exploring for geothermal resources with electromagnetic methods. *Surveys In Geophysics, 35*(1), 101–122.

Noorollahi, Y., Jamaledini, M. R., & Ghazban, F. (1998). *Geothermal potential areas in Iran*. Tehran: Renewable Energy Organization of Iran (SUNA).

Nouraliee, J., & Ebrahimi, D. (2012). *Geochemical studies in Mahallat Geothermal Region*, Internal Report [in Persian]. Niroo Research Institute (NRI), Tehran, Iran.

Nouraliee, J., Porkhial, S., Mohammadzadeh-Moghaddam, M., Mirzaei, S., Ebrahimi, D., & Rahmani, M. R. (2015). Investigation of density contrasts and geologic structures of hot springs in the Markazi Province of Iran using the gravity method. *Russian Geology and Geophysics, 56*(12), 1791–1800.

Oskooi, B., & Darijani, M. (2014). 2D inversion of the magnetotelluric data from Mahallat geothermal field in Iran using finite element approach. *Arabian Journal of Geosciences, 7,* 2749–2759.

Oskooi, B., Darijani, M., & Mirzaie, M. (2013). Investigation of electrical resistivity and geological structure on the hot springs in Markazi province of Iran using magnetotelluric method. *Bollettino di Geofisica ed Applicata, 54,* 245–256.

Oskooi, B., Mirzaei, M., Mohammadi, B., Mohammadzadeh-Moghaddam, M., & Ghadimi, F. (2016). Integrated interpretation of the magnetotelluric and magnetic data from Mahallat geothermal field, Iran. *Studia Geophysica et Geodaetica, 60*(1), 141–161.

Oskooi, B., Pedersen, L. B., Smirnov, M., Arnasson, K., Esteinsson, H., Manzella, A., et al. (2005). The deep geothermal structure of The Mid-Atantic Ridge deduced from MT data in SW Iceland. *Physics of the Earth and Planetary Interiors, 150,* 183–195.

Paoletti, V., Di Maio, R., Cella, F., Florio, G., Motschka, K., Roberti, N., et al. (2009). The Ischia volcanic island (Southern Italy): Inferences from potential field data interpretation. *Journal of Volcanology and Geothermal Research, 179,* 69–86.

Patro, P. K. (2017). Magnetotelluric studies for hydrocarbon and geothermal resources: Examples from the Asian region. *Surveys In Geophysics, 38,* 1005–1041.

Peng, C., Pan, B., & Xue, L. (2019). Geophysical survey of geothermal energy potential in the Liaoji Belt, northeastern China. *Geothermal Energy, 7,* 14.

Porkhial, S., Nouraliee, J., Rahmani, M., & Ebrahimi, D. (2013). Resource assessment of Vartun geothermal region, central Iran. *Journal of Tethys, 1,* 29–40.

Ravat, D. (1996). Analysis of the Euler method and its applicability in environmental magnetic investigations. *Journal of Environmental and Engineering Geophysics, 1*(3), 229–238.

Reid, A. B., Allsop, J. M., Granser, H., Millett, A. T., & Somerton, I. W. (1990). Magnetic interpretation in three dimensions using Euler deconvolution. *Geophysics, 55*(1), 80–91.

Rezaei, A., Javadi, H., Rezaeian, M., & Barani, S. (2018). Heating mechanism of the Abgarm–Avaj geothermal system observed with hydrochemistry, geothermometry, and stable isotopes of thermal spring waters, Iran. *Environmental Earth Sciences, 77*(18), 635.

Rezaie, M., Ghorbani, M., & Bomeri, M. (2009). The hydrogeology and geothermology of the Mahallat hot springs. In *1st national conference on hydrogeology, Behbehan, Iran*, Extended Abstract, 4 pp.

Richards, J., Wilkinson, D., & Ullrich, T. (2006). Geology of the Sari Gunay epithermal gold deposit, Northwest Iran. *Economic Geology, 101,* 1455–1496.

Ritz, J. F., Nazari, H., Salamati, R., Shafeii, A., Solaymani, S., & Vernant, P. (2006). Active transtension inside central Alborz: A new insight into the northern Iran-southern Caspian geodynamics. *Geology, 34,* 477–480.

Rodi, W., & Mackie, R. L. (2001). Nonlinear conjugate gradients algorithm for 2-D magnetotelluric inversion. *Geophysics, 66*(1), 174–187.

Spichak, V., & Manzella, A. (2009). Electromagnetic sounding of geothermal zones. *Journal of Applied Geophysics, 68*(4), 459–478.

SUNA. (1998). *Country Geothermal Potential Survey*. 1st Phase Report to the Renewable Energies Office, Ministry of Energy, Islamic Republic of Iran, 306 pp.

Thompson, D. T. (1982). EULDPH a new technique for making computer-assisted depth estimates from magnetic data. *Geophysics, 47,* 31–37.

Thurston, J. B., & Brows, R. J. (1992). The filtering characteristics of least-squares polynomial approximation for regional/residual separation. *Canadian Journal of Exploration Geophysics, 28*(2), 71–80.

Yazdi, M., Hassanvand, M., Tamasian, O., & Navi, P. (2016). Hydrogeochemical characteristics of Mahallat hot springs, central Iran. *Journal of Tethys, 4*(2), 169–179.

Yoder, H. S. (2015). *Evolution of the igneous rocks: Fiftieth anniversary perspectives*. Princeton: Princeton University Press.

Yousefi, H., Noorollahi, Y., Ehara, S., Itoi, R., Yousefi, A., Fujimitsu, Y., et al. (2010). Developing the geothermal resources map of Iran. *Geothermics, 39,* 140–151.